SUPPORTING INFORMATION for

Phonon engineering in twinning superlattice nanowires

Marta De Luca, Claudia Fasolato, Marcel A. Verheijen, Yizhen Ren, Milo Y. Swinkels, Sebastian Kölling, Erik P. A. M. Bakkers, Riccardo Rurali, Xavier Cartoixà, and Ilaria Zardo

Supporting Information 1: Structural investigation

In order to demonstrate that all the investigated TSLs NWs exhibit very similar structural characteristics, Supplementary Figure 1 (panels 1a and 1b) shows TEM images (top panels) taken on two NWs different from the one described in Figure 1 in the main text, along with the extracted variation of the period (2L) along the NW length (bottom panels). Panel 1c shows the period variation of three additional wires. In all the NWs, at the NW tip (position = 0 μm) there is a segment with 2L between 24 and 48 nm, followed by a transition region with 2L between 25 and 10 nm, followed by final segment with constant period of about 8-12 nm.

We have determined the period length along all investigated NWs by using BF images taken by tilting the NW slightly off the <110> zone axis (~1° around <11-1> and <2-11> axes). In this way, the characteristic alternating contrast of darker and brighter stripes (see, for instance, Supplementary Figure 1a) representing domains of alternating orientations was obtained, owing to the fact that one type of domain is strongly diffracting, while the other type is not. Then, the length of the alternating domains was extracted from the images by creating a brightness profile along the NW and calculating the distance between two subsequent peaks in the brightness profile.

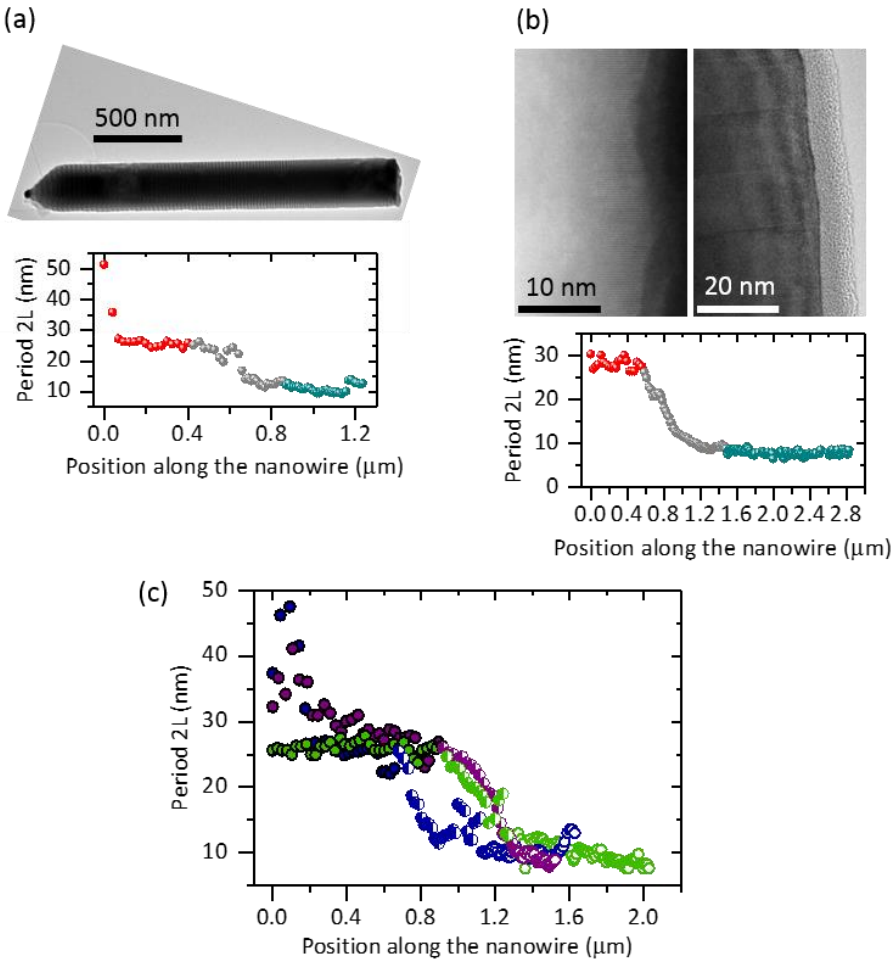

Supplementary Figure 1. a BF TEM image of a whole typical TSL NW and relative extracted period along the NW. **b** HAADF STEM images acquired on another NW (near the tip, left panel; near the bottom, right panel) and extracted period lengths. In the bottom panels, different colors highlight the different period regions along the NW. **c** Variation of period along the length of three different NWs (indicated by the three colors). Filled symbols highlight the long period region, half-filled symbols the transient period region, empty symbols the short period region.

Supporting Information 2: Computed Spectra

Since in a III-V semiconductor the phonon frequencies at Γ depend on the direction from which Γ is approached, for each calculated phonon mode we obtain slightly different frequencies and intensities for nonequivalent non-analyticities at Γ, which in turn result in different Raman spectra. All the theoretical Raman spectra shown in the main text have been computed taking into account the proper non-analytical corrections (NACs) suitable to the specific scattering geometry, as detailed below. Since all our measurements were performed with k_i and k_s along

x, the momentum exchanged between photons and phonons is along *x*, and thus all theoretical spectra in the main text are calculated with NAC along *x*. In Supplementary Figure 2 we show the different Raman spectra that are generated when all NACs are averaged (thick lines) or when only the right NAC are considered (thin lines) for WZ (a) and TSL (b) NWs. Clearly, averaging among all NACs induces forbidden modes, as the LO, to appear, so it is important to consider the proper NAC. However, we point out that in Raman experiments on NWs selection rules are often partially relaxed (see more details in Supporting Information 5), and therefore calculating spectra where all NAC are averaged can be a useful operation to qualitatively estimate the effect of relaxed selection rules.

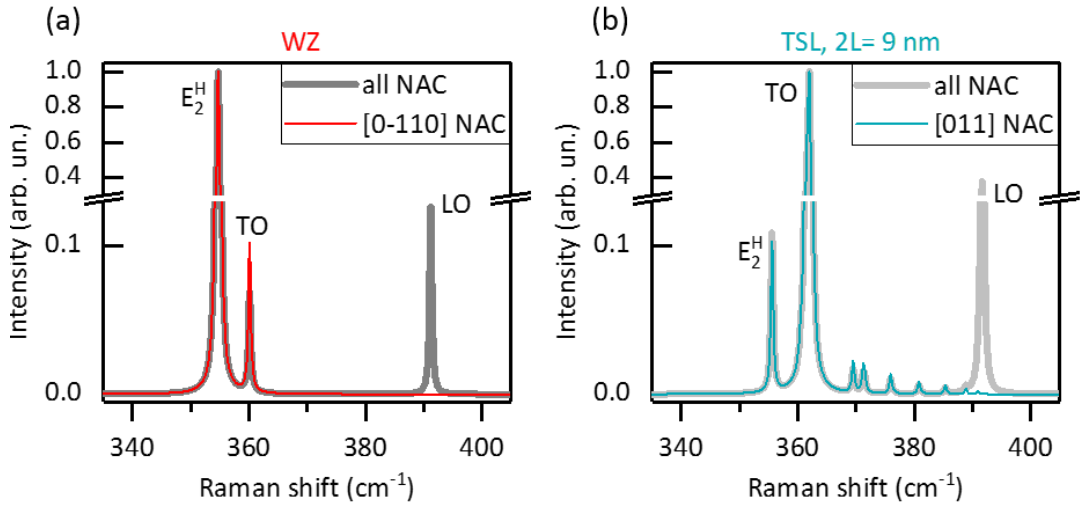

Supplementary Figure 2. Calculated Raman spectra in the $\bar{x}(yy)x$ configuration on GaP WZ (**a**) and TSL with period of 9 nm (**b**) with all NAC (thick lines) and with the proper NAC (thin lines). All spectra are normalized to the TO mode. The fwhm of each mode is set to 0.5 cm^{-1} (much smaller than in the experiment: here it was chosen to highlight the NAC effect on all the peaks, also those very close to the LO mode).

Supporting Information 3: Effect of microscope numerical aperture on selection rules

In order to estimate the influence of the microscope objective on optical selection rules, we have investigated the bulk GaP sample, where the absence of tilted facets typical of NWs allows for a clean and reliable evaluation of this purely optical effect. Supplementary Figure 3a displays the Raman spectra acquired on the cleaved (011) GaP surface lying on the *yz* plane

with a 100x objective (NA=0.95, thin line) and with a 20x objective (NA=0.4, thick line). The power density is different due to different spot sizes, and the ensuing different signals are thus normalized to the TO mode. In the spectrum acquired with the 20x objective the intensity of the LO mode is almost zero, which renders the spectrum very similar to the calculated one displayed in panel 3b, where the LO mode is forbidden by selection rules because the photon wavevectors are assumed to be parallel to x[1,2]. In the experiment, the forbidden LO mode becomes more and more visible as the NA of the objective increases because a higher NA implies a higher density of photons with wavevector tilted with respect to the x axis and thus having a component in the yz plane. In the top parts of Supplementary Figure 3 we report a sketch of this effect: the green light cone is meant to represent the ensemble of all wavevectors impinging on (and collected after the scattering by) the sample. The angle between the x axis (dashed line) and the most tilted wavevector in the cone is given.

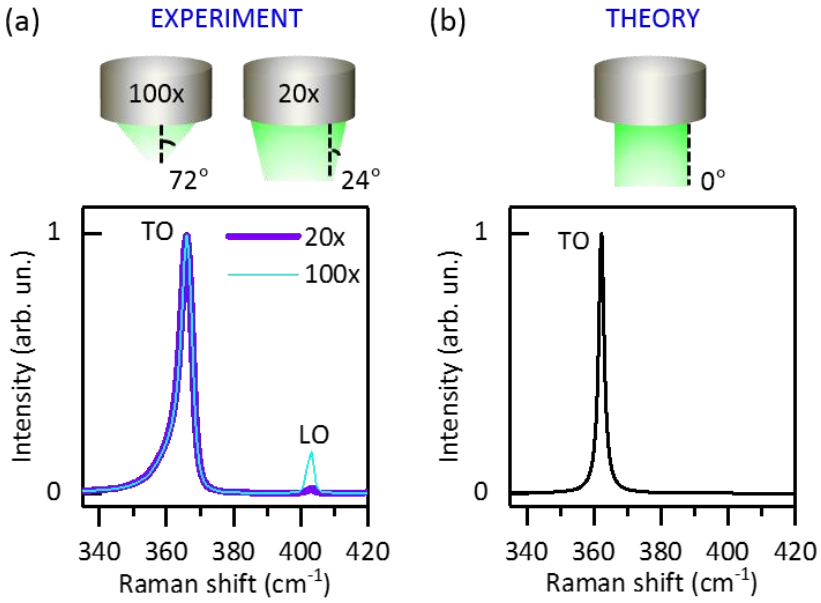

Supplementary Figure 3. a Experimental Raman spectra (bottom) collected on GaP bulk in $\bar{x}(zz)x$ scattering geometry with two different objectives (20x, thick line; 100x, thin line) and sketch (top) of the effect of their NA on the tilting of the photon wavevectors: the angle α between the vertical x direction (dashed line) and the most tilted wavevector in the light cone is given in degrees (calculated by NA=n sin α, where n=1 is the air refractive index). **b** Calculated Raman spectrum in $\bar{x}(zz)x$ configuration (bottom) in the ideal case (sketched on top) of objective with NA=0 and thus wavevectors directed along x.

Supporting Information 4: Lineshape of phonon modes in experimental Raman spectra of GaP

In the experimental Raman spectra of all the GaP samples (ZB bulk, WZ and TSL NWs), we observe a considerable asymmetry in the lineshape of the TO mode, while the LO lineshape is symmetric. The asymmetric broadening of the TO mode on the low-energy side has been ascribed in bulk GaP to an anharmonic interaction of the TO phonon with a nearly degenerate band of two-phonon acoustic states[3,4,5]. In Ref. 3, the Raman spectrum of GaP has been fitted with the optical response of three oscillators (i.e., three vibrational resonances) featuring frequency-dependent damping. In order to reduce the number of free parameters as much as possible, we have resorted to a simpler fitting procedure to be applied to both reference and TSL spectra. The low-frequency broadening of the TO has been reproduced with an asymmetric Breit-Wigner-Fano (BWF) function, usually employed to fit lineshapes resulting from a coupling of discrete excitations with a quasi-continuum of states[6,7]: as we are trying to reproduce the spectral shape of a single phonon at a discrete energy (the TO mode) coupling with a broad spectral feature in the two-phonon density of states, the use of a BWF lineshape is well justified. To fully account for the TO mode lineshape, we have used a Voigt function (namely, a convolution of Gaussian and Lorentzian), due to the peculiar anharmonicity of GaP. For consistency, we used a Voigt function also for the LO mode, though it exhibits mostly a Lorentzian character. The result for the bulk case is reported in Supplementary Figure 4. The lineshape of all the other peaks different from TO and LO in the TSL and WZ NWs is Lorentzian, if not differently specified.

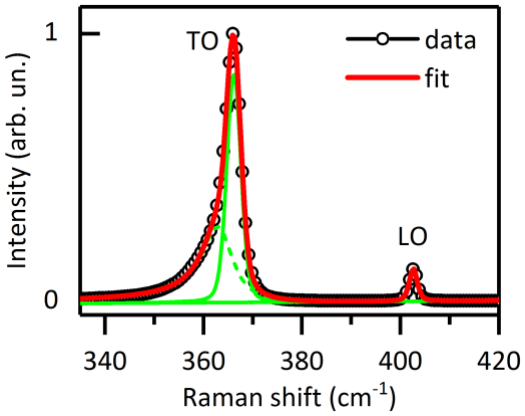

Supplementary Figure 4. Raman spectrum (open circles) collected on GaP bulk in $\bar{x}(yy)x$ configuration fitted with three curves (displayed in green thin lines): a Voigt function and a slightly asymmetric BWF function (dashed line) account for the lineshape of the TO peak, and a Voigt function (with mostly Lorentzian character) accounts for the lineshape of the LO. The sum of the curves results in the thick red line.

Supporting Information 5: Selection Rules

In this section we explain why the $\bar{x}(yy)x$ scattering configuration is the most appropriate to detect the TSL-originated Raman modes. Supplementary Figure 5a-c shows the calculated Raman spectra of a TSL crystal with 9 nm period in the three main scattering configurations introduced in Section III of the main text. In panel 5a, the three spectra resulting from the procedure explained in the Computational Methods and in the Supporting Information 2 are displayed. In panel 5b they are magnified to show more clearly the TSL modes (E_2^H and modes between TO and LO). Since in NWs there are several effects responsible for a relaxation of selection rules (the effect of the NA, present also in the bulk, and additional size effects present only in nanostructures), the relative intensity between Raman signals collected in different configurations can be different from the theoretical one. In panel 5c, where the three calculated spectra are normalized to the TO mode, the enhancement of the TSL modes in the $\bar{x}(yy)x$ scattering configuration can be appreciated. Furthermore, the E_2^H mode is slightly visible in $\bar{x}(zy)x$, and the TSL modes between TO and LO are slightly visible in $\bar{x}(zz)x$.

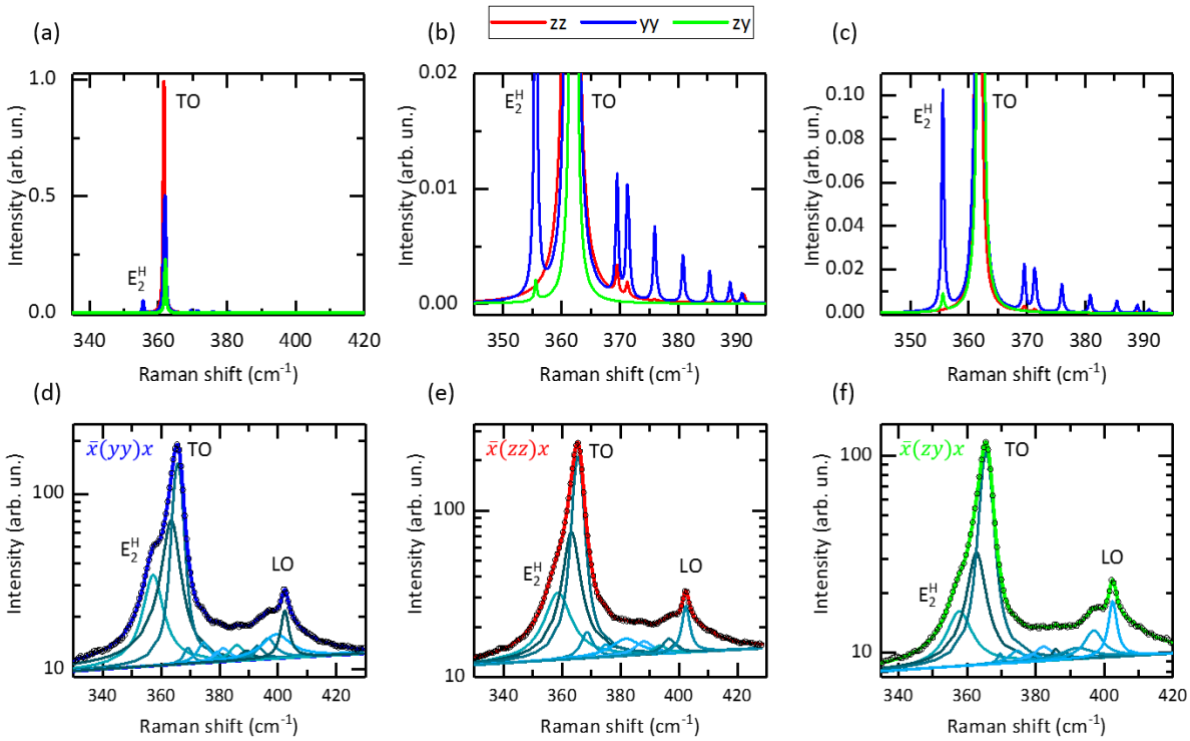

Supplementary Figure 5. a-c Calculated Raman spectra in the $\bar{x}(zz)x$ (red), $\bar{x}(yy)x$ (blue), and $\bar{x}(zy)x$ (green) configurations on GaP TSL with period of 9 nm and NAC along the ZB <011>. The fwhm of each mode is 0.5 cm^{-1}, much smaller than the experimental one, for clarity reasons. Panel **a** shows the intensities as obtained from the calculations, in panel **b** the three spectra are zoomed in both *x* and *y* axis to highlight the TSL peaks, and panel **c** shows a zoom of the three spectra which have been normalized to the TO mode. **d-f** Raman spectra (open circles) measured on a TSL NW with period length of ~9 nm in the indicated geometries. Deconvoluted components of the data fitting are displayed by thin lines, resulting fits by thick lines. The intensity scale is logarithmic to allow for a better visibility of the spectral features.

We have collected Raman spectra also in $\bar{x}(zz)x$ and $\bar{x}(zy)x$ configurations to have a qualitative estimation of the relaxation of selection rules in TSL NWs, see Supplementary Figure 5d-f. The TO mode is maximum in $\bar{x}(zz)x$, decreases in $\bar{x}(yy)x$, and further decreases in $\bar{x}(zy)x$. This is in qualitative agreement with the prediction in Supplementary Figure 5a, though the quantitative difference between the three experimental spectra is smaller than in the theoretical ones. The TSL-related modes are more clearly visible and more intense in $\bar{x}(yy)x$ (especially the E_2^H) than in the other two configurations, as predicted by theory. The relative intensity between E_2^H and the modes between TO and LO in $\bar{x}(yy)x$ is also in good agreement

with the theory. However, in the experimental spectra all the TSL modes are visible also in the other two configurations. The visibility of the E_2^H mode is quite affected by the asymmetric shape of the TO due to anharmonicity; indeed, at 5.5 K, the selection rules of this mode are satisfied (see Supplementary Figure 9). The modes between TO and LO suffer from a stronger disagreement with selection rules, even at 5.5 K. Therefore, we ascribe this to a relaxation of selection rules and not to anharmonicity. In particular, the high NA could make forbidden modes appear, similarly to what happens to the LO. Moreover, size effects are not considered in the calculations of selection rules, which are obtained for a bulk TSL crystal. In our NWs the diameter is approximately an order of magnitude smaller than the NW length and the period length is another order of magnitude smaller than the diameter. As a result, we expect size effects to be non-negligible.

Supporting Information 6: Raman Spectra collected at opposite nanowires' ends

The variation of the period along the NWs allows probing the phonon modes of TSLs with quite different periods within a same NW. Supplementary Figure 6 displays Raman spectra collected at two opposite NW ends (2L= 9 nm *vs* 2L=26 nm) in $\bar{x}(yy)x$. Due to an increase in the period length by almost a factor of three going from the NW bottom to the tip, the number of atoms in the unit cell increases accordingly, and so does the number of back-folded TSL phonon modes. Similarly to what is discussed in Figure 3a, the intensity of those modes is thus expected to decrease. Supplementary Figure 6 clearly shows that a shorter period corresponds indeed to a more intense E_2^H mode and more intense spectral features between TO and LO, as expected. Regarding the number of phonon modes, it is not possible to prove that there are many more TSL modes in the longer period part than in the shorter one, as it is not possible to perform a quantitative analysis of the long period part by including ~20 TSL modes between TO and LO without introducing a non-negligible degree of arbitrariness (the analysis performed including the minimum number of peaks is in panel b). This fact sets an upper limit to the detectability of

the *number* of TSL modes at period lengths of about 15-20 nm, while their decrease in *intensity* is clear also at longer period lengths.

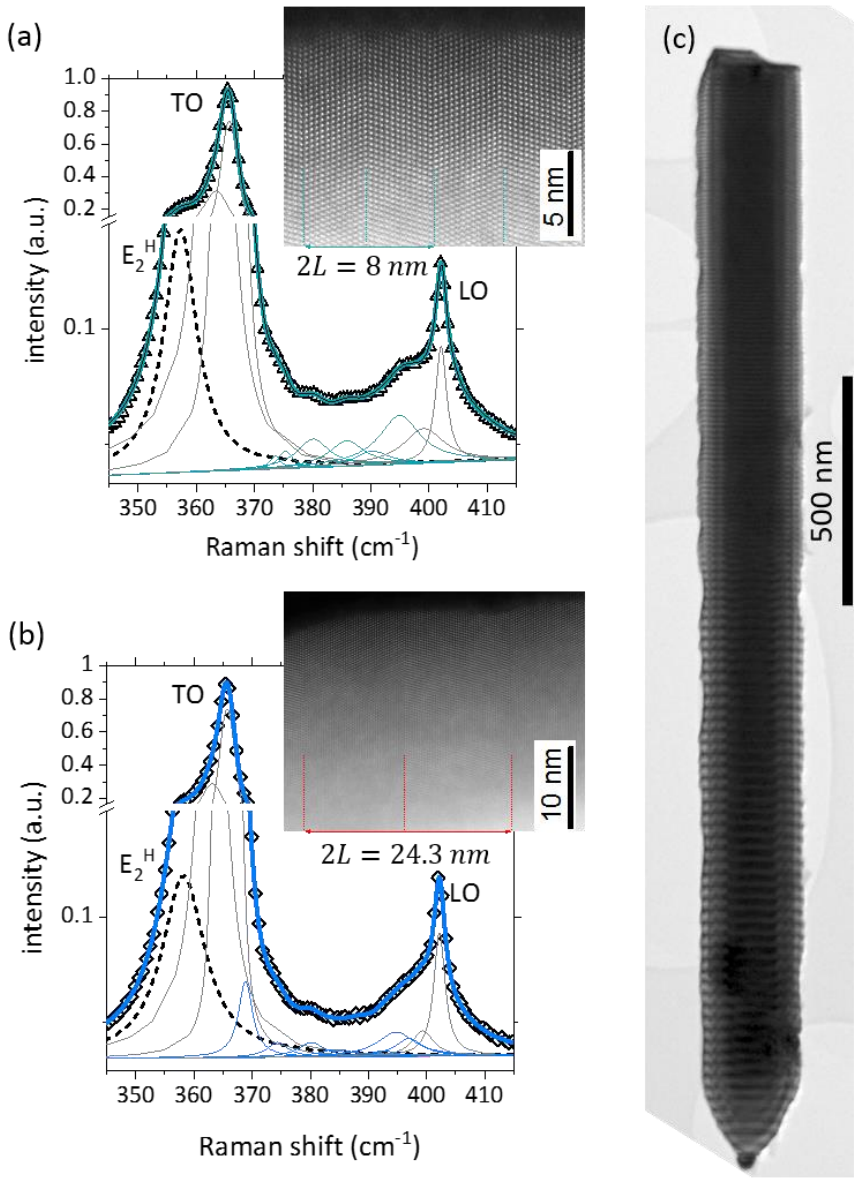

Supplementary Figure 6. a Measured spectrum of a GaP TSL with ~9 nm period length. Deconvoluted components of the data fitting are displayed. The measurement was performed on the TSL NW whose HAADF TEM image is shown in the inset (2L= 8 nm in the inset because the TEM image is taken at the very bottom, while laser spot probes on average a region with 9 nm period). **b** Same as in **a** for a NW part with ~26 nm period length (2L= 24.3 nm in the inset because the TEM image is taken at the very top, while laser spot probes on average a region with 26 nm period). Spectra displayed in **a** and **b** where collected at two ends of the nanowire whose BF TEM image is shown in **c**.

Supporting Information 7: Raman Spectra of different nanowires

In Figure 3 and 4 in the main text we have demonstrated that tuning the TSL period allows tuning the characteristics of the phonon modes arising from the superlattice structure. To show that we have found results similar to those displayed in Fig. 3 b and c in the main text and in Supplementary Figure 6 in all the investigated TSL NWs, in Supplementary Figure 7 we display Raman spectra collected at opposite NW ends on three different NWs (shown in the three different rows), along with the deconvoluted components of the data fitting (thin lines) and the resulting fits (thick lines). In all the NWs, we observe more intense and clearer TSL modes (E_2^H mode and the modes between TO and LO) in the regions of short periods, as predicted by theory.

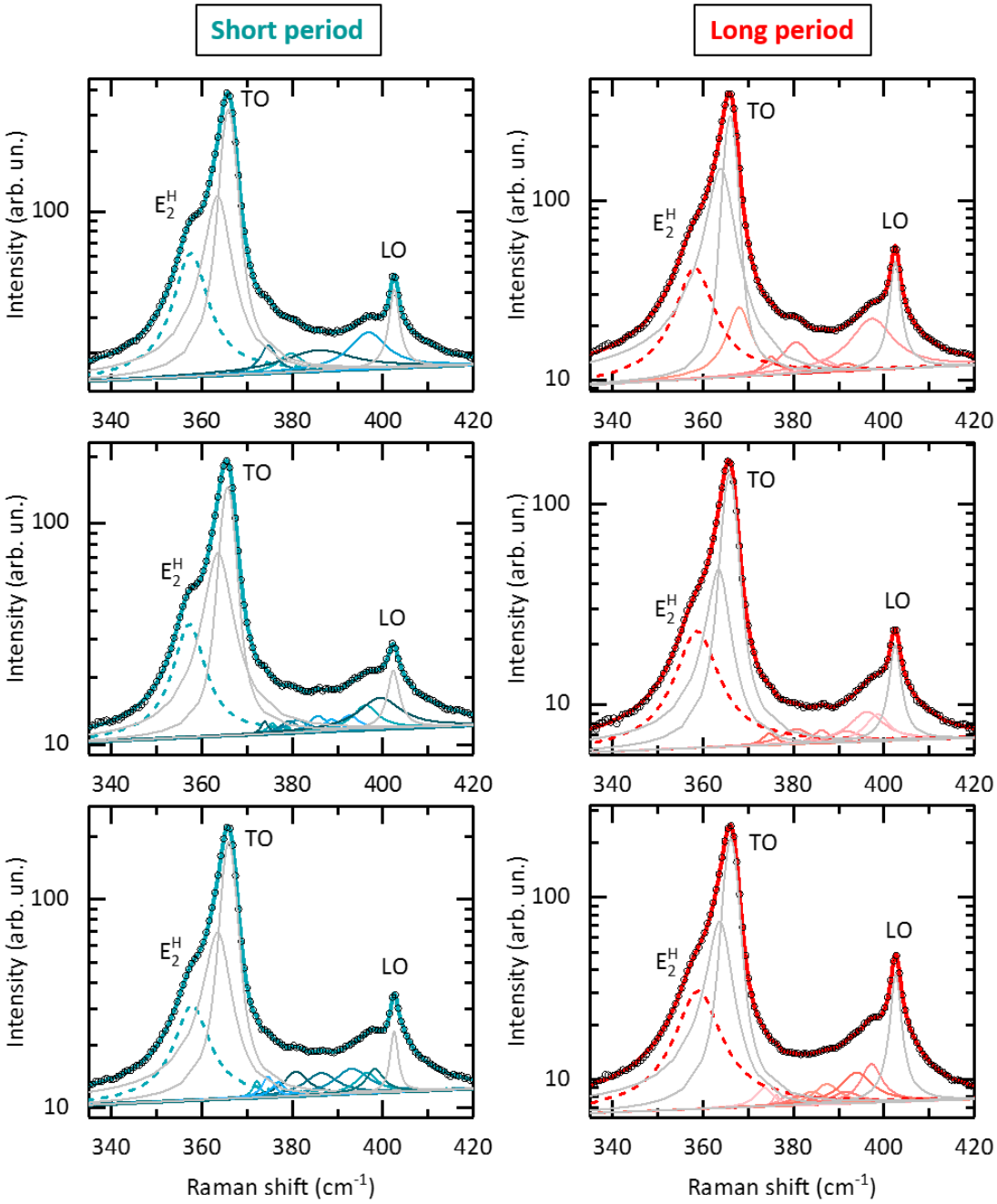

Supplementary Figure 7. Measured Raman spectra (open circles) of three GaP twin superlattice NWs (different rows are relative to different NWs) taken on two opposite NW ends: the one with short period (10±2 nm, left column) and the one with long period (31±5 nm, right column). The spectrum displayed for the short period part of the NW in the second (third) row is also shown in Figure 2c (3c) in the main text. Deconvoluted components of the data fitting are displayed by thin lines (colored lines indicate peaks arising from the twin superlattice structure –among which the E_2^H is shown by a dashed line– and by the SO mode, while grey lines indicate phonon modes typical of any GaP sample). Resulting fits are displayed by thick lines. All spectra were recorded in the $\bar{x}(yy)x$ configuration.

Supporting Information 8: Raman Spectra collected with different excitation wavelengths

Supplementary Figure 8 displays deconvoluted Raman spectra collected on the short period part of two different NWs with two excitation wavelengths (~515 nm, left column; ~633 nm, right column) and same power (0.35 mW). The spectra collected with 633 nm are characterized by narrower lineshapes (due to a higher spectral resolution) and lower signal (due to a lower setup efficiency) compared to the spectra collected with the 515 nm. Besides this, there is no significant difference between the two data sets: indeed, regardless of the excitation wavelength, we observe clear TSL modes (E_2^H mode and the modes between TO and LO), as predicted by theory. This is a confirmation that the TSL modes are intrinsic to the NW crystal structure, similarly to the TO and LO modes, and are not arising because of peculiar experimental conditions. The similarity between the results collected with two wavelengths holds as well for spectra collected on the opposite NW ends.

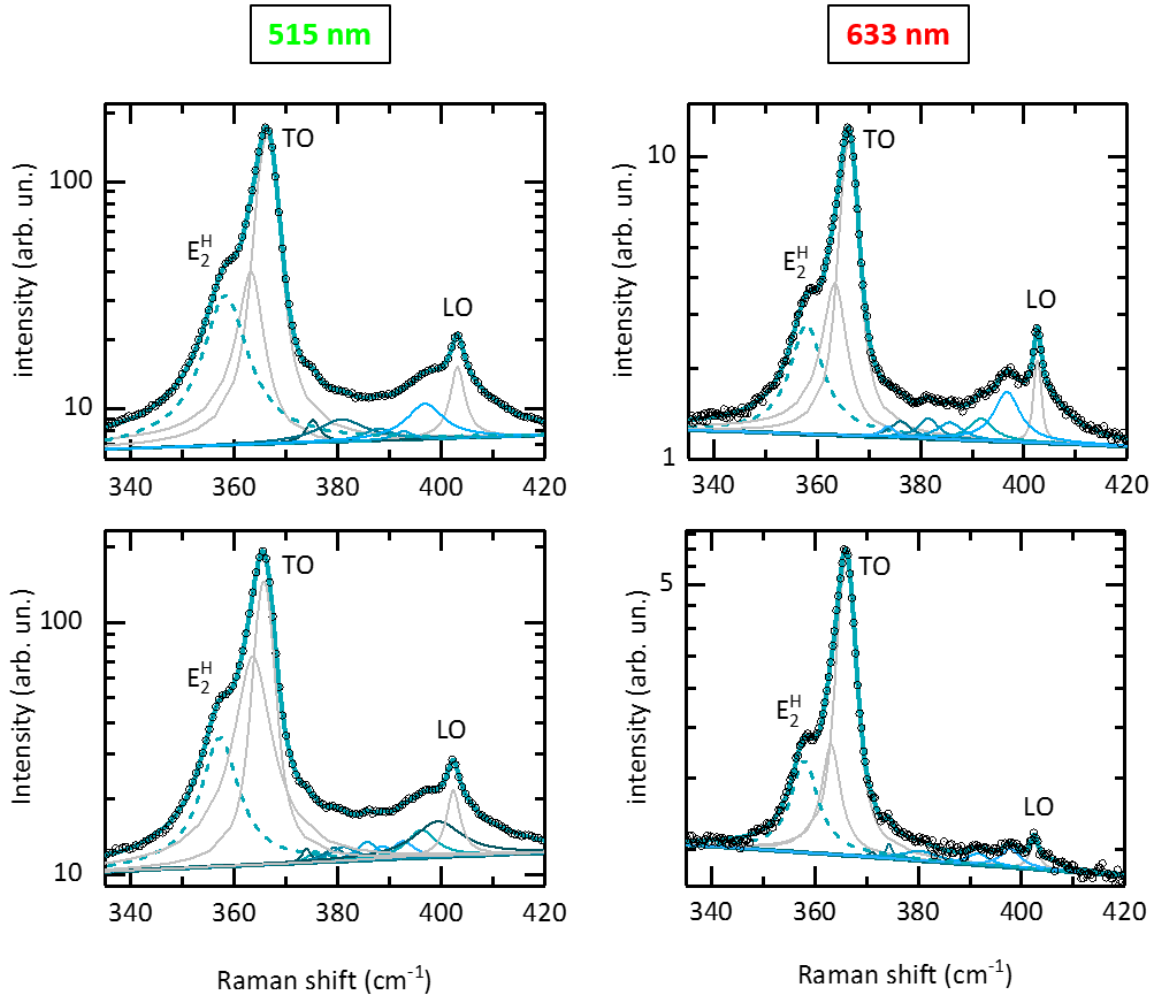

Supplementary Figure 8. Measured Raman spectra (open circles) of two GaP twin superlattice NWs (different rows are relative to different NWs) taken on the NW part having short period (10±2 nm) with two different excitation wavelengths (514.5 nm, left column; 632.8 nm, right column) in $\bar{x}(yy)x$. Deconvoluted components of the data fitting are displayed by thin lines (colored lines indicate peaks arising from the twin superlattice structure –among which the E_2^H is shown by a dashed line– while grey lines indicate phonon modes typical of any GaP sample). Resulting fits are displayed by thick lines.

Supporting Information 9: Low-Temperature measurements

All the experimental results collected at room temperature are reproduced also in the spectra collected at 5.5 K, which are displayed in Supplementary Figure 9 for a NW whose RT spectra are shown in the first row of Supplementary Figure 7. In particular, spectra in the first row of Supplementary Figure 9 are taken in the same scattering configuration, $\bar{x}(yy)x$, and on the same NW points (having either short or long period) as the ones in Supplementary Figure 7, so they are directly comparable: in both cases, the phonon modes arising from the superlattice

structure (both the E_2^H and the modes between TO and LO) are more intense and clear in the part with the short period, as predicted by theory. This is particularly evident for the E_2^H peak (black thick line). The second and the third rows show spectra collected in $\bar{x}(zz)x$ and $\bar{x}(zy)x$ scattering geometries, respectively. The relative intensities between the spectra collected in the different geometries is very similar to the ones obtained at RT (see Supplementary Figure 5d-f), and thus not completely agreeing with the predicted selection rules due to the three effects discussed in Supporting Information 5. However, the decrease in temperature enables a decrease in the anharmonicity effects that render the TO lineshape asymmetric, and therefore allows for a more reliable estimation of the intensity of the E_2^H peak. Indeed, at variance with the RT spectra, in the 5 K spectra there is no E_2^H mode in $\bar{x}(zz)x$, as predicted by theory, and there is a small E_2^H peak $\bar{x}(zy)x$, whose intensity is higher in the short period region, as expected.

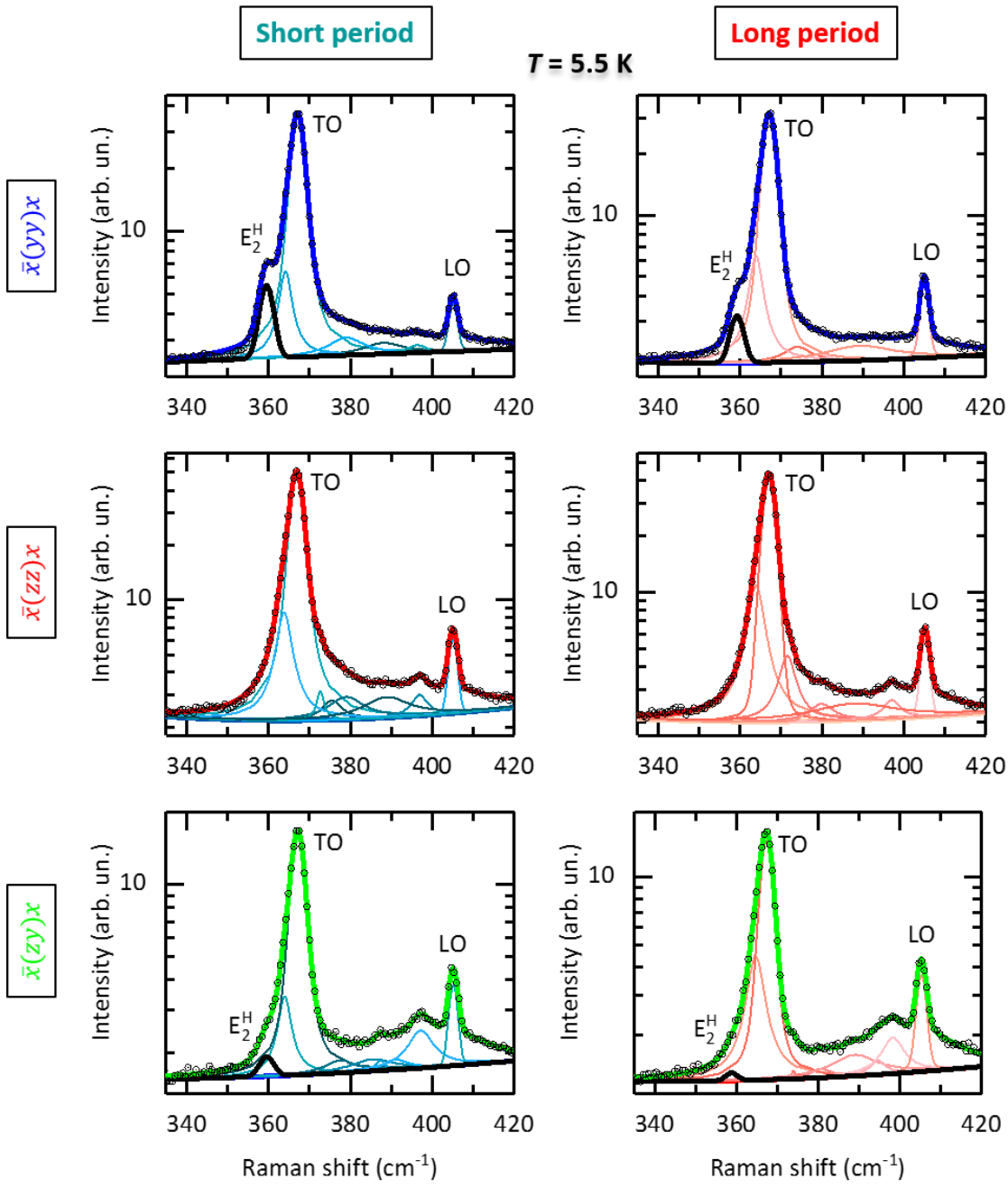

Supplementary Figure 9. Low-temperature (5.5 K) Raman spectra (open circles) of the GaP twin superlattice NW (see first row in Figure S8 for RT spectra) collected on two opposite NW ends: the one with short period (10±2 nm, left column) and the one with long period (31±5 nm, right column). Deconvoluted components of the data fitting are displayed (the E_2^H is shown by a thick black line), along with resulting fits. Spectra were recorded in the indicated scattering configurations.

Supporting Information 10: Backfolded low frequency modes

In this section we show that the calculations demonstrate that also acoustic modes undergo the same folding as optical modes. Since the $\bar{x}(yy)x$ scattering configuration is the most appropriate to detect the TSL-originated Raman modes, Supplementary Figure 10 shows the calculated Raman spectrum of a TSL crystal with 9 nm period in the $\bar{x}(yy)x$ scattering configuration. In the left panel, the spectrum resulting from the procedure explained in the Computational Methods and in the Supporting Information 2 is displayed. In the middle and right panels, the spectrum is magnified to show more clearly the TSL modes arising from the backfolding of the acoustic modes. These modes are not visible in the experimental TSL spectrum only because their intensity is two to three orders of magnitude lower than e.g. the E_2^H mode intensity.

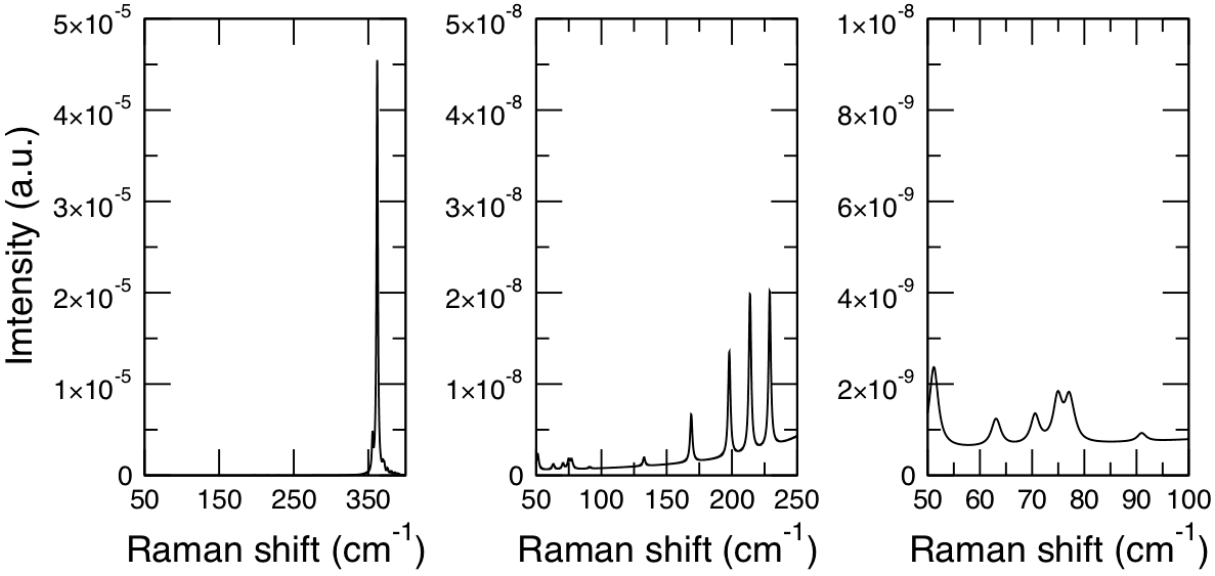

Supplementary Figure 10. Calculated Raman spectrum in the $\bar{x}(yy)x$ configuration on GaP TSL with period of 9 nm. The fwhm of each mode is 2 cm^{-1}. The left panel shows the intensities as obtained from the calculations, in the middle panel the spectrum is zoomed to highlight the backfolded TSL peaks between 100 and 250 cm^{-1}, and in the right panel shows a zoom of the spectrum to highlight the backfolded modes between 50 and 100 cm^{-1}.

References

[1] M. Cardona, R. K. Chang, G. Güntherodt, M.B. Long, H. Vogt, *Light Scattering in Solids II, Topics in Applied Physics, Eds.*, Springer, Germany (1982).

[2] A. Cantarero, *Review on Raman scattering in semiconductor nanowires: I. theory*, J. of Nanophotonics **7**, 071598 (2013).

[3] A. S. Barker, Jr., *Dielectric Dispersion and Phonon Line Shape in Gallium Phosphide*, Phys. Rev. **165**, 917 (1968).

[4] B. A. Weinstein, *Pressure dependent optical phonon anharmonicity in GaP*, Solid State Commun. **20**, 999 (1976).

[5] F. Widulle, T. Ruf, A. Göbel, E. Schönherr, and M. Cardona, *Raman Study of the Anomalous TO Phonon Structure in GaP with Controlled Isotopic Composition*, Phys. Rev. Lett. **82**, 5281 (1999).

[6] M. Balkanski, K. P. Jain, R. Beserman, and M. Jouanne, *Theory of interference distortion of Raman scattering line shapes in semiconductors*, Phys. Rev. B **12**, 4328 (1985).

[7] C. Jiang, K. Kempa, J. Zhao, U. Schlecht, U. Kolb, T. Basché, M. Burghard, and A. Mews, *Strong enhancement of the Breit-Wigner-Fano Raman line in carbon nanotube bundles caused by plasmon band formation*, Phys. Rev. B **66**, 161404 (2002).